

Continuous phase-space representations for finite-dimensional quantum states and their tomography

Bálint Koczor,^{1,2,3,*} Robert Zeier,^{1,4,†} and Steffen J. Glaser^{1,2,‡}

¹Technical University of Munich, Department of Chemistry, Lichtenbergstrasse 4, 85747 Garching, Germany

²Munich Center for Quantum Science and Technology (MCQST), Schellingstrasse 4, 80799 München, Germany

³University of Oxford, Department of Materials, Parks Road, Oxford OX1 3PH, United Kingdom

⁴Forschungszentrum Jülich GmbH, Peter Grünberg Institute,
Quantum Control (PGI-8), 52445 Jülich, Germany

(Dated: November 2, 2019)

Continuous phase spaces have become a powerful tool for describing, analyzing, and tomographically reconstructing quantum states in quantum optics and beyond. A plethora of these phase-space techniques are known, however a thorough understanding of their relations was still lacking for finite-dimensional quantum states. We present a unified approach to continuous phase-space representations which highlights their relations and tomography. The infinite-dimensional case from quantum optics is then recovered in the large-spin limit.

I. INTRODUCTION

Phase spaces provide both theoretically and experimentally useful ways to visualize and analyze abstract states of infinite- and finite-dimensional quantum systems. A plethora of phase-space representations are known [1–4], including the Glauber P, Wigner, and Husimi Q function, each of which has provided insights in quantum optics, quantum information theory, and beyond. Phase spaces have also played an essential role in characterizing the quantum nature of light and became a natural language for quantum optics due to the seminal work of Glauber [5–7], also clarifying their interrelations in terms of Gaussian convolutions. Beyond quantum optics, phase spaces are conceptually invaluable and provide a complete description of quantum mechanics. They mirror and naturally reduce to classical phase spaces in the limit of a vanishing Planck constant [8–13]. Phase-space techniques and their associated quantizations [14–16] have been widely applied in the context of harmonic analysis and pseudo-differential operators [17–21]. In this work, we focus on *finite-dimensional* quantum states, for which phase-space methods have been explored only to a lesser extent.

Recent advances in experimentally creating entangled quantum states for spins or spin-like systems, such as atomic ensembles [22, 23], Bose-Einstein condensates [24–32], trapped ions [33–35], and light polarization [36–38], have been in certain cases illustrated with phase-space techniques and therefore call for a more profound understanding of these tools with regard to finite-dimensional quantum states. To this end, we present a general approach to continuous phase spaces for spins which clarifies their interrelations by conveniently translating between them, while emphasizing the connection

to the infinite-dimensional case from quantum optics. We do not consider discrete phase spaces such as the one proposed by Wootters [39], see also [40–42] and references therein.

Phase-space representations have become crucial in the tomographic reconstruction of infinite-dimensional quantum states [1, 43]. The optical homodyne tomography reconstructs the quantum state of light by directly measuring the planar Radon transform of the Wigner function [43, 44]. Also, the Husimi Q function [45] has been experimentally measured for various systems [23, 32, 34, 36, 46–48]. We detail how to tomographically reconstruct a class of finite-dimensional phase-space representations.

In this work, we develop a general and unified description of continuous phase-space representations for quantum states of a single spin with arbitrary, integer or half-integer spin number J (i.e. a qudit with $d = 2J+1$), which is simultaneously applicable to experimental bosonic systems consisting of indistinguishable qubits [50–53]. A single qudit can be identified with a bosonic system consisting of $2J$ indistinguishable qubits: Figure 1 depicts a quantum state of a single qudit (i.e. a single spin J) corresponding to a (generalized) W state [54] (i.e. Dicke state) of $2J$ indistinguishable qubits (see also Sec. III A of [51] for an explicit map and Chap. 3.8 of [55] or [56] for links to the second quantization). In particular, we address the following fundamental open questions related to finite-dimensional phase-space representations (e.g., Glauber P, Wigner, and Husimi Q): (a) How can they be systematically defined to naturally recover the infinite-dimensional case of quantum optics in the limit of large J ? (b) How can they be transformed into each other? (c) How can their experimental tomographic approaches be formulated in a unified way?

We present answers to these questions for the full class of (finite-dimensional) s -parametrized phase-space representations with $-1 \leq s \leq 1$. Our approach relies on rotated parity operators and thereby significantly simplifies earlier work (such as [57] and particular cases discussed

* balint.koczor@materials.ox.ac.uk

† r.zeier@fz-juelich.de

‡ glaser@tum.de

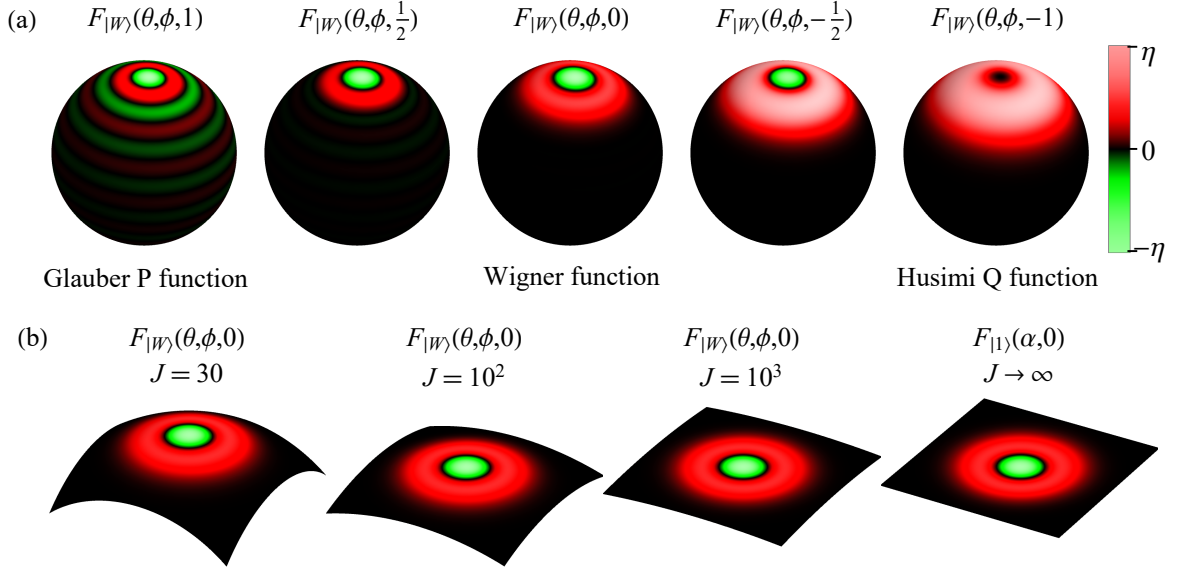


FIG. 1. (a) s -parametrized phase-space representations $F_{|W\rangle}(\theta, \phi, s)$ for $s \in \{1, 1/2, 0, -1/2, -1\}$ of a (generalized) W state $|W\rangle$ for a single spin with $J = 10$, or equivalently the symmetric Dicke state $|J, J-1\rangle$ of $2J$ indistinguishable qubits with a single Majorana vector pointing to the south pole and $2J-1$ vectors pointing to the north pole. A decreasing s (left-to-right) which smears out $F_{|W\rangle}(\theta, \phi, s)$ is interpreted as a Gaussian-like convolution. Red (dark gray) and green (light gray) represent positive and negative values, respectively. The brightness reflects the absolute value of the function relative to its global maximum η . (b) Spherical Wigner functions $F_{|W\rangle}(\theta, \phi, 0)$ for increasing J approach their planar counterpart, i.e., the single-photon state $F_{|1\rangle}(\alpha, 0)$ (see Sec. II). Identical coordinate patches with $-1.2 \leq x, y \leq 1.2$ have been used, where $x = R \sin \theta \cos \phi$, $y = R \sin \theta \sin \phi$ in the first three plots and $x = \Re(\alpha)$, $y = \Im(\alpha)$ in the last one. (For the plots in (b), methods from [49] to efficiently approximate phase-space representations for large J have been applied.)

in [58, 59]). It also extends [60–64] in the case of single spins (and bosonic systems consisting of indistinguishable qubits) to all s -parametrized phase spaces. In addition to a deeper theoretical knowledge connecting planar and spherical phase spaces, the insights provided here will also guide practitioners to design innovative experimental schemes, such as the tomographic reconstruction of phase-space representations. Before discussing finite-dimensional quantum states, we first review important properties of the infinite-dimensional phase spaces from quantum optics.

II. SUMMARY OF INFINITE-DIMENSIONAL PHASE-SPACE REPRESENTATIONS

Let us recall the s -parametrized phase-space distribution function (where $-1 \leq s \leq 1$)

$$F_\rho(\Omega, s) = \text{Tr}[\rho \mathcal{D}(\Omega) \Pi_s \mathcal{D}^\dagger(\Omega)] \quad (1)$$

as the expectation value of the parity operator Π_s (*vide infra*) transformed by the displacement operator $\mathcal{D}(\Omega)$, which acts on coherent states via $\mathcal{D}(\Omega)|0\rangle = |\Omega\rangle$ [65], refer also to [7, 17, 43, 66]. We have developed and discussed the theoretical foundations for the case of infinite dimensions considered in formula (1) in Ref. [67], while building on earlier work by Grossmann [68] for Wigner

functions. Here, $|0\rangle$ denotes the vacuum state and Ω fully parametrizes a phase space with either the variables p and q or the complex eigenvalues α of the annihilation operator [5, 43].

Different parity operators Π_s lead to different distribution functions $F_\rho(\Omega, s)$. The Q function $Q_\rho = Q_\rho(\Omega) := F_\rho(\Omega, -1)$ arises from the parity operator Π_{-1} whose entries are given by $[\Pi_{-1}]_{nn} := \delta_{n0}$ [66] in the number state representation [43]. Similarly, the Wigner function $W_\rho := F_\rho(\Omega, 0)$ is determined by $[\Pi_0]_{nn} = 2(-1)^n$ [66], which inverts phase-space coordinates via $\Pi_0|\Omega\rangle = |-\Omega\rangle$ [17]. The P function $P_\rho := F_\rho(\Omega, 1)$ is singular for all pure states [7], and the entries of its parity operator Π_1 diverge in the number-state representation [66]. The discussed representations are considered in the upper part of Fig. 2. An example is given by the vacuum state $|0\rangle$ whose Wigner function $W_{|0\rangle} = 2e^{-2|\alpha|^2}$ is a Gaussian distribution. The respective Q function $Q_{|0\rangle} = e^{-|\alpha|^2}$ is a Gaussian of double width and the P function is the two-dimensional delta function $P_{|0\rangle} = \delta^{(2)}(\alpha)$.

We now recollect how to transform between phase-space representations with Gaussian convolutions [7, 43]. Two phase-space distribution functions $K(\Omega)$ and $F(\Omega)$ can be combined using their convolution [43]

$$[K * F](\Omega) = \int [\mathcal{D}^{-1}(\Omega)K(\Omega')]F(\Omega') d\Omega', \quad (2)$$

which corresponds to a multiplication in the Fourier do-

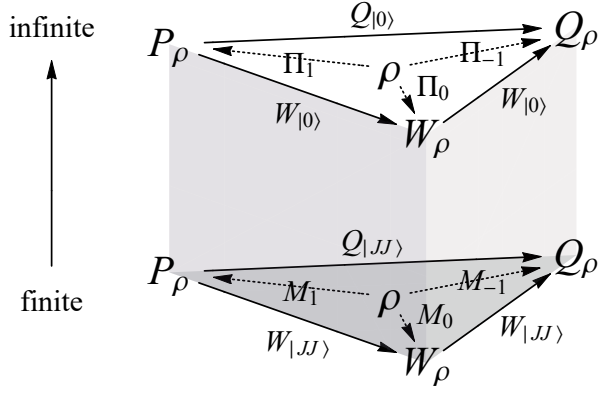


FIG. 2. Phase-space representations W_ρ , Q_ρ , P_ρ of *infinite*- or *finite*-dimensional density operators ρ as expectation value of parity operators Π_s or M_s [dashed arrows], see Eqs. (1) or (4). Transformed by Gaussian smoothing with $W_{|0\rangle}$, $Q_{|0\rangle}$ or reversibly with $W_{|JJ\rangle}$, $Q_{|JJ\rangle}$ [solid arrows], see Eqs. (3) or (10).

main. Convolution of a distribution function $F_\rho(\Omega, s)$ with the vacuum-state representation $F_{|0\rangle}(\Omega, s')$ results in the phase-space distribution function

$$F_\rho(\Omega, s+s'-1) = F_{|0\rangle}(\Omega, s') * F_\rho(\Omega, s) \quad (3)$$

of type $s+s'-1$. A convolution $P_{|0\rangle}(\Omega) * F(\Omega) = F(\Omega)$ with the P function $P_{|0\rangle}$ acts as an identity operation, while a convolution with the Gaussians $W_{|0\rangle}$ or $Q_{|0\rangle}$ blurs out $F_\rho(\Omega, s)$. This Gaussian smoothing is widely used in image processing and allows us to transform different phase-space representations into each other [43] as in the upper part of Fig. 2. For example, the non-negative Q function $Q_\rho = W_{|0\rangle} * W_\rho$ is obtained from the Wigner function W_ρ by convolution with $W_{|0\rangle}$; the negative regions in W_ρ are therefore bounded by the variance $1/4$ of $W_{|0\rangle}$ [43].

III. PHASE-SPACE REPRESENTATIONS FOR SPINS

A. Definition of phase-space representations for spins

We establish a consistent formalism for s -parametrized phase-space representations ($-1 \leq s \leq 1$) for quantum states of single spins, which in the limit of an increasing spin number J converges to the just discussed infinite-dimensional case. The continuous phase space $\Omega := (\theta, \phi)$ can be completely parametrized in terms of two Euler angles of the rotation operator $\mathcal{R}(\Omega) = \mathcal{R}(\theta, \phi) := e^{i\phi\mathcal{J}_z}e^{i\theta\mathcal{J}_y}$, where \mathcal{J}_z and \mathcal{J}_y are components of the angular momentum operator [69]. The rotation operator $\mathcal{R}(\Omega)$ replaces the displacement operator $\mathcal{D}(\Omega)$ and maps the spin-up state $|JJ\rangle$ to spin coherent states $|\Omega\rangle = \mathcal{R}(\Omega)|JJ\rangle$ [59, 65, 70, 71]. This leads to a spherical phase space, whose radius is set to $R := \sqrt{J/(2\pi)}$.

Result 1. For a density operator ρ of a single spin J , the s -parametrized phase-space representation [cf. Eq. (1)]

$$F_\rho(\Omega, s) := \text{Tr}[\rho \mathcal{R}(\Omega) M_s \mathcal{R}^\dagger(\Omega)] \quad (4)$$

is the expectation value of the rotated parity operator

$$M_s := \frac{1}{R} \sum_{j=0}^{2J} \sqrt{\frac{2j+1}{4\pi}} (\gamma_j)^{-s} T_{j0}, \quad (5)$$

which is a weighted sum of zeroth-order tensor operators.

In Result 1, the diagonal tensor operators $[T_{j0}]_{mm'} = \delta_{mm'} \sqrt{(2j+1)/(2J+1)} C_{Jm,j0}^{Jm}$ of order zero [72] have been applied in Eq. (5), and they can be specified via the Clebsch-Gordan coefficients $C_{Jm,j0}^{Jm}$ [69] where $j \in \mathbb{N} \cup \{0\}$ and $m, m' \in \{-J, \dots, J\}$. We also use the coefficients $\gamma_j := R \sqrt{4\pi} (2J)! [(2J+j+1)! (2J-j)!]^{-1/2}$. With increasing spin number J , the parity operators M_s converge to the infinite-dimensional operators Π_s in Eq. (1), refer to [73, Theorem 2.1] for a proof, while rotations transform into translations along the tangent of a sphere [59, 71, 74, 75]. The phase-space representations in Eq. (4) fulfill the Stratonovich postulates [57, 58, 76–78]; an s -parametrized version is given in Ref. [57]. Prior results [60–64] using rotated parity operators are extended for single spins to all s -parametrized phase spaces. For Wigner functions, our definition conforms to [64] but differs from Eq. (8) in [62]. The latter can be identified as a linearly shifted Q function $aQ_\rho - b$, and it relaxes the postulate $\text{tr}(AB) = \int_{S^2} F_A(\Omega, 0) F_B(\Omega, 0) d\Omega$. We consider in this work only spherical rotations (even for qudits) which yield spherical phase spaces, forgoing general rotations [61–63, 79]. Generalizations to coupled spins are known in the Wigner case [62, 63, 80]; our methods in [78] are also applicable.

We further highlight how the approach of Result 1 connects to earlier work. An equivalent form of the s -parameterized phase-space representation in Eq. (4) has been previously determined in Eq. (5.28) of [57] (up to a global factor) as

$$F_\rho(\Omega, s) = \text{Tr}[\rho \Delta_s(\theta, \phi)], \quad (6)$$

$$\text{with } \Delta_s(\theta, \phi) := \frac{1}{R} \sum_{j=0}^{2J} \sum_{m=-j}^j (\gamma_j)^{-s} T_{jm} [Y_{jm}(\theta, \phi)]^*$$

using the kernel $\Delta_s(\theta, \phi)$. Here, $[Y_{jm}(\theta, \phi)]^*$ denotes the complex conjugate of $Y_{jm}(\theta, \phi)$. The work of [57, 81] builds on the particular cases of $s \in \{-1, 0, 1\}$ obtained in [77]. Along similar lines, the pioneering work of [58] proposed spherical-harmonics expansions (see Eq. (3.15) in [58]) for spin phase-space representations

$$F_\rho^{(\Omega)}(\theta, \phi) = \sum_{j=0}^{2J} \sum_{m=-j}^j c_{jm}^{(\Omega)} Y_{jm}(\theta, \phi), \quad (7)$$

which are indexed by $\Omega = \Omega_{jm}$ and use the coefficients $c_{jm}^{(\Omega)} = \text{Tr}[\rho T_{jm}^\dagger] / \Omega_{jm}$. For s -parametrized phase spaces,

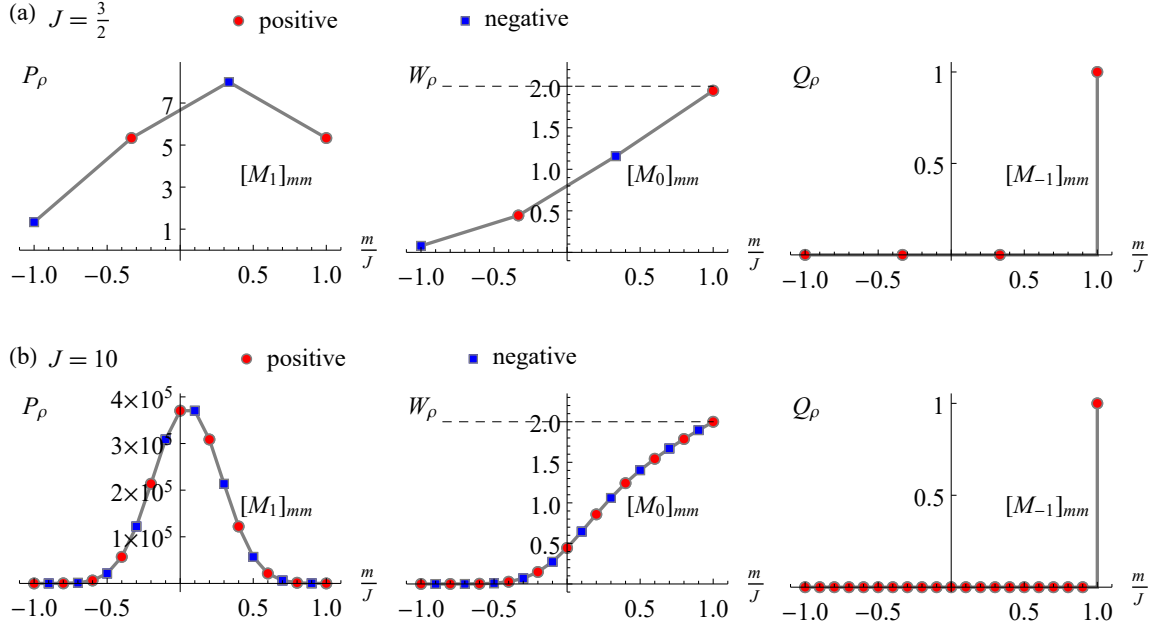


FIG. 3. Parity-operator entries $[M_s]_{mm}$ corresponding to Eq. (5) [and equivalently the Stern-Gerlach reconstruction weights in Eq. (12)] for a single spin J shown for the P function P_ρ , the Wigner function W_ρ , and the Q function Q_ρ .

one has $\Omega = \Omega_{jm} = R\gamma_j^s$. Note that [58] established the explicit form of Ω_{jm} only for Husimi Q functions, i.e., $s = -1$. The case of Wigner functions ($s = 0$) has been discussed in [59]. Note that the tensor-operator components T_{jm} can be explicitly given as $[T_{jm}]_{m_1 m_2} = \sqrt{(2j+1)/(2J+1)} C_{Jm_2, jm}^{Jm_1} = (-1)^{J-m_2} C_{Jm_1, J-m_2}^{jm}$ using Clebsch-Gordan coefficients and $m_1, m_2 \in \{J, \dots, -J\}$ [57, 69, 82, 83].

By using rotated parity operators, the approach of Result 1 has important conceptual advantages when compared to Eqs. (6)-(7). First, Result 1 separates the dependence on the parameter s in the parity operator from the rotations. Second, Eq. (4) naturally transforms in the large-spin limit into the infinite-dimensional case discussed in Eq. (1) by replacing rotations $\mathcal{R}(\Omega)$ with displacements $\mathcal{D}(\Omega)$. Third, the above mentioned tensor operators and spherical-harmonics decompositions are averted and the rotations $\mathcal{R}(\Omega)$ can be efficiently calculated via the Wigner D-matrix [84, 85]. Finally, the particular form given in Result 1 enables us to develop general tomography formulas in Sec. IV below.

Particular cases of Result 1 are considered in the lower part of Fig. 2. The Q function specifies the expectation value of rotated spin-up states, where $[M_{-1}]_{mm} := \delta_{mJ}$ (right of Fig. 3), and its zeros are the so-called Majorana vectors [36, 86, 87]. The Wigner function determines the expectation value of the rotated parity operator M_0 . The matrix entries $[M_0]_{mm}$ are shown in the middle of Fig. 3, highlighting their infinite-dimensional limit of ± 2 for $m/J \approx 1$ [74]. The matrix entries $[M_1]_{mm}$ for the parity operator of the P function are shown in the left panel of Fig. 3, including their rapid divergence.

Further exploring the infinite-dimensional limit of large J , the phase-space representation

$$F_{|JJ\rangle}(\theta, s) := \frac{1}{R^2} \sum_{j=0}^{2J} \sqrt{\frac{2j+1}{4\pi}} (\gamma_j)^{1-s} Y_{j0}(\theta) \quad (8)$$

of the spin-up state (i.e. the ground state with least uncertainty) is easily expanded into a weighted sum of axially symmetric spherical harmonics $Y_{j0}(\theta)$. The examples $Q_{|JJ\rangle}$, $W_{|JJ\rangle}$, and $P_{|JJ\rangle}$ are plotted in Fig. 4 as functions of the angle θ . Even though the Gaussian width of $F_{|JJ\rangle}(\theta, s)$ shrinks in terms of θ with increasing J , $F_{|JJ\rangle}(\theta, s)$ converges to the Gaussian $F_{|0\rangle}(\Omega, s)$ related to the infinite-dimensional vacuum state if parametrized by the relevant arc length $a := \theta R = \theta \sqrt{J/(2\pi)}$ (Fig. 1(b) illustrates the sphere-to-plane transition in the infinite-dimensional limit).

For example, $Q_{|JJ\rangle}$ is equal to the Wigner D-matrix element $|D_{JJ}^J|^2 = \cos(\theta/2)^{4J}$, and it converges rapidly with increasing J to the Gaussian $Q_{|0\rangle}(\alpha) = e^{-|\alpha|^2} = e^{-a^2\pi} = e^{-J\theta^2/2}$ using the phase-space coordinate $\alpha = \sqrt{\pi}ae^{-i\phi}$ [70, 71]. Similarly, $W_{|JJ\rangle}$ rapidly converges to the normalized Gaussian $W_{|0\rangle} = 2e^{-2|\alpha|^2} = 2e^{-2a^2\pi} = 2e^{-J\theta^2}$ of the vacuum state. The P function $P_{|JJ\rangle}(\theta) := \tilde{\delta}(\Omega)$ is the spherical *sinc* function, i.e., a truncated version of the spherical delta function $\delta(\Omega) := \delta(\theta)\delta(\phi)/\sin\theta$ (where the tilde projects onto the physical subspace of spherical harmonics with rank $j \leq 2J$ [88]), which by definition approaches the delta function in the large-spin limit $\delta(\Omega) := \sum_{j=0}^{\infty} \sqrt{(2j+1)/(4\pi)} Y_{j0}(\Omega)$. Qualitative similarities between certain finite- and infinite-dimensional Wigner functions were already highlighted in [59]. But

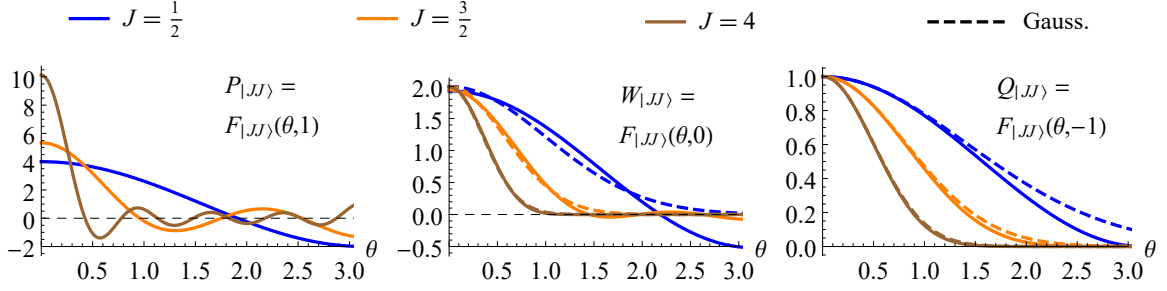


FIG. 4. Phase-space representations $F_{|JJ\rangle}(\theta, s)$ of the spin-up state $|JJ\rangle$, c.f. Eq. (8). As J increases, $Q_{|JJ\rangle}$ and $W_{|JJ\rangle}$ rapidly converge to the Gaussian distributions $Q_{|0\rangle}$ and $W_{|0\rangle}$ (dashed line); $P_{|JJ\rangle}$ slowly approaches the delta function $P_{|0\rangle} = \delta(\Omega)$.

this connection is clarified in our formulation by emphasizing the large-spin convergence for all of the s -parametrized phase spaces, refer to [73, Theorem 2.1] for a proof.

B. Spherical convolution

To translate between the different spherical phase-space representations in the lower part of Fig. 2 (which can be done reversibly assuming arbitrary precision), we define the convolution [cf. Eq. (2)]

$$[K * F](\Omega) := \int_{S^2} [\mathcal{R}^{-1}(\Omega)K(\Omega')]F(\Omega') d\Omega' \quad (9)$$

via a spherical integration where $d\Omega' = R^2 \sin \theta' d\theta' d\phi'$. First, the kernel function $K(\Omega')$ is rotated by $\mathcal{R}^{-1}(\Omega)$ to $K(\Omega' - \Omega)$, which is then projected onto the distribution function $F(\Omega')$ via a spherical integral. The kernel function $K(\Omega')$ has to be axially symmetric due to the so-called Funk-Hecke theorem [89, 90]. The spherical convolution is a multiplication in the spherical-harmonics domain, and substituting spherical harmonics into Eq. (9) yields $Y_{j'0} * Y_{jm} = R^2 \sqrt{4\pi/(2j+1)} Y_{jm} \delta_{jj'}$. This allows us to transform between different spherical phase-space representations:

Result 2. *The convolution of a phase-space distribution function $F_\rho(\Omega, s)$ with the phase-space representation $F_{|JJ\rangle}(\Omega, s')$ of the spin-up state results in a type- $(s+s'-1)$ distribution function [cf. Eq. (3)]*

$$F_\rho(\Omega, s+s'-1) = F_{|JJ\rangle}(\theta, s') * F_\rho(\Omega, s). \quad (10)$$

The pioneering work of [58] proposed spin phase-space representations in the form of spherical-harmonics expansions [refer to Eq. (7)] and defined their relations using integral transformation kernels (see (3.19) in [58]). Result 2 clarifies that these relations are in fact spherical convolutions, in complete analogy with the infinite-dimensional case considered in quantum optics. The general form of Eq. (10) has not been formally described in the literature before. Some convolution properties were detailed for *discrete*, planar phase spaces in [91, 92]. We want

to also stress that spherical convolutions have efficient implementations [93, 94].

In the infinite-dimensional limit of an increasing spin number J , Eq. (10) turns into Eq. (3). We emphasize that the convolution transformation in Eq. (10) is reversible (assuming arbitrary precision) for general parameters $s, s' \in \mathbb{R}$ (as the coefficients γ_j in Eq. (8) are non-zero). Also, a convolution $P_{|JJ\rangle}(\theta) * F(\Omega, s) = F(\Omega, s)$ with the P function $P_{|JJ\rangle}(\theta)$ acts as an identity operation, just as in the infinite-dimensional case. The Wigner function W_ρ can be transformed into the non-negative Q function $Q_\rho = W_{|JJ\rangle} * W_\rho$ by Gaussian-like smoothing, cf. Fig. 1. Consequently, the negative regions of W_ρ are bounded by the variance $\propto 1/4$ of $W_{|JJ\rangle}$, similar as for infinite-dimensional phase spaces. Result 2 completes our characterization of how to transform between spherical phase-space representations as illustrated in Fig. 2.

C. Examples of phase-space functions

Figure 5 depicts phase-space representations of typical finite-dimensional quantum states. The P, Wigner, and Q functions are shown in a triangular arrangement along with their corresponding convolution kernels, which generate the spherical convolutions from Eq. (10) between edges of the triangle.

In Fig. 5(a), we consider the quantum state of a single spin J corresponding to the $2J$ -qubit GHZ state $|\text{GHZ}\rangle = (|0\rangle^{\otimes 2J} + |1\rangle^{\otimes 2J})/\sqrt{2} = (|JJ\rangle + |J, -J\rangle)/\sqrt{2}$ consisting of a quantum superposition of the two symmetric Dicke states given by the spin-up and spin-down state (which can be identified with a $2J$ -photon NOON state). This GHZ state factorizes up to permutations into a product of its Majorana vectors $\otimes_k |v_k\rangle$ [86, 87], where $|v_k\rangle$ is a single-qubit state with Bloch vector v_k . These Majorana vectors correspond to zeros of the Q function and point to the edges of a regular n -gon, see $Q_{|\text{GHZ}\rangle}$ in Fig. 5(a). The zeros of the Q function can (e.g.) be determined by spherically convolving the Wigner function with the convolution kernel $W_{|JJ\rangle}$ (cf. Sec. III B), and the negative (green) lobes of $P_{|\text{GHZ}\rangle}$ and $W_{|\text{GHZ}\rangle}$ in Fig. 5(a) identify the direction of the Majorana vectors. The Q

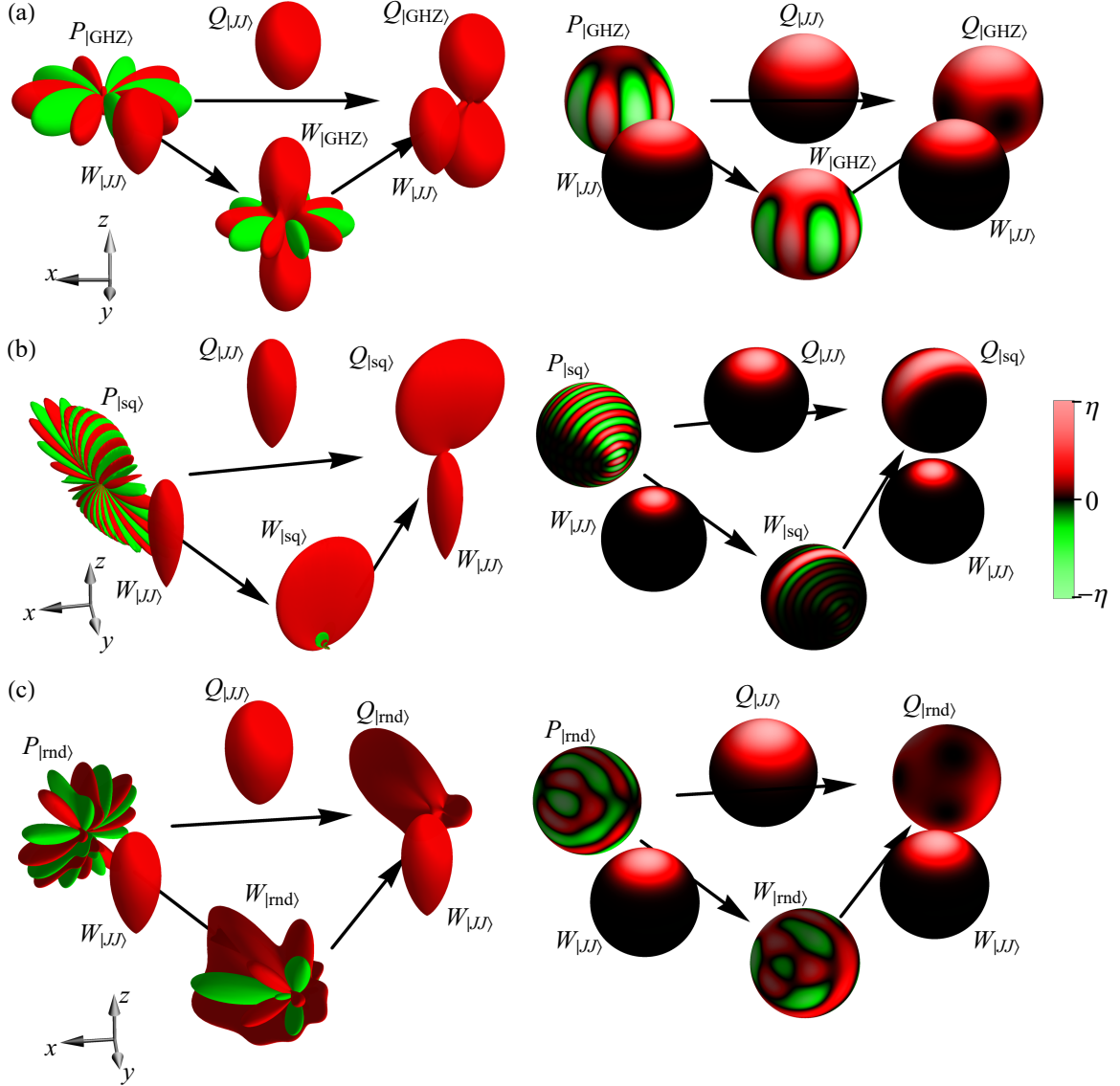


FIG. 5. P, Wigner, and Q functions with their corresponding convolution kernels for (a) a quantum state of a spin $J = 5/2$ corresponding to the GHZ state $|\text{GHZ}\rangle$ of $2J$ indistinguishable qubits, (b) a squeezed state $|\text{sq}\rangle$ of a spin $J = 10$, and (c) a random state $|\text{rnd}\rangle$ of a spin $J = 4$ [95] (see Sec. III C). Red (dark gray) and green (light gray) represent positive and negative values, respectively. The absolute values of the spherical function relative to its global maximum η is given by the plotted surface (left) or the brightness (right), where each variant highlights different properties of the plotted functions.

function largely resembles the classical superposition of a spin-up and a spin-down state, but has a five-fold symmetry.

Figure 5(b) shows phase-space plots of the squeezed state $\exp[-i\theta \mathcal{I}_y^2/2]|JJ\rangle$ with squeezing angle $\theta := 0.3$ for a single spin with spin number $J = 10$, where the state is squeezed along the y axis [96]. A random pure state of a single spin with spin number $J = 4$ is depicted in Fig. 5(c).

IV. TOMOGRAPHY

A. Pointwise tomography of phase-space functions

We detail how phase-space representations are recovered from Stern-Gerlach experiments assuming that a chosen density operator ρ can be prepared identically and repeatedly. In a single Stern-Gerlach experiment, one detects the density matrix ρ in a projection eigenstate according to a reference frame rotated by Ω (i.e., by rotating the measurement device or inversely rotating ρ). For repeated Stern-Gerlach experiments, measured

frequencies converge to the Stern-Gerlach probabilities

$$p_m(\Omega) = \langle Jm | \mathcal{R}^\dagger(\Omega) \rho \mathcal{R}(\Omega) | Jm \rangle. \quad (11)$$

In the limiting case of infinite-dimensional parity operators [67, 73, 74], this is known in quantum optics as the ‘direct measurement’ technique [97–100]. Here, we have the finite-dimensional equivalent:

Result 3. *The phase-space representations*

$$F_\rho(\Omega, s) = \sum_{m=-J}^J [M_s]_{mm} p_m(\Omega) \quad (12)$$

of a $(2J+1)$ -dimensional quantum state ρ are directly determined for each phase-space point Ω by the probability distributions $p_m(\Omega)$ of repeated Stern-Gerlach experiments, see Eq. (11). The weights $[M_s]_{mm}$ are given by the parity operator from Eq. (5).

The pointwise tomography of Result 3 has not been described in this generality before. We discuss different cases of the parameter s by referring to the examples of phase-space functions in Fig. 5. In particular, the P functions P_{GHZ} , P_{sq} , and P_{rnd} in Fig. 5 show considerable detail, while mostly utilizing probabilities $p_m(\Omega)$ of small $|m|$ (cf. Fig. 3). The Wigner functions W_{GHZ} , W_{sq} , and W_{rnd} in Fig. 5 require all $2J+1$ Stern-Gerlach probabilities $p_m(\Omega)$ [22, 29, 30, 63, 101] and show fewer detail consistent with being smoothed versions of the corresponding P functions. Finally, the Q functions show little detail due to a second Gaussian smoothing (yet low-rank contributions would still be recognizable [23, 30, 32, 34, 53]) and are fixed by the probability $p_J(\Omega)$ of the spin-up state [48]. Certain features of our tomography approach such as the weights in Eq. (12) are invariant under slight variations of a sufficiently large spin number J , and this might be useful in atomic ensembles [22, 23], Bose-Einstein condensates [24, 25, 27–30], or trapped ions [33–35].

We detail how Result 3 is applied in the estimation of the s -parametrized phase-space function $F_\rho(\Omega, s)$ of a quantum state ρ at a single phase-space point $\Omega = (\theta, \phi)$: the quantum state is rotated according to the angles (θ, ϕ) , a projective Stern-Gerlach measurement is performed, the measured eigenstate m is recorded, and the whole procedure is repeated N_r times. Then the probabilities $p_m(\theta, \phi)$ can be estimated from the relative frequencies N_m/N_r of the eigenstates, where the eigenstate m has been recorded N_m times during the measurements. This enables the reconstruction of a phase-space function at the phase-space point (θ, ϕ) as a linear combination of the estimated probabilities in Eq. (12), where the weights $[M_s]_{mm}$ are illustrated in Fig. 3. The Wigner-function tomography for a random ensemble of $N_\rho = 2200$ spin-5/2 states (which are distributed with respect to the Hilbert-Schmidt distance [102]) has been simulated with $N_r = 10^2$, 10^3 , and 10^4 repetitions for the phase-space point $(\theta, \phi) = (0, 0)$ and for each reconstructed random state. Figure 6 (a) shows the reconstruction errors which

follow an empirical Gaussian (i.e. normal) distribution. The standard deviation empirically scales with $N_r^{-1/2}$ and therefore vanishes as the number N_r of repetitions increases. We now apply the pointwise tomography first for multiple phase-space points and then to obtain a full tomography of a phase-space function.

B. Pointwise tomography for multiple phase-space points

The pointwise tomography of Result 3 can be easily repeated for multiple phase-space points. This enables an *approximate* pointwise reconstruction of phase-space functions: the approximation improves as the number of phase-space points increases. Figure 6 (b) shows the average error of pointwisely reconstructed phase-space functions, and this average error reduces as the number of Stern-Gerlach measurements increases. However, this approximation has a notably discrete flavor as it only recovers a phase-space function at the chosen phase-space points and not between them. In Sec. IV C below, we detail a measurement strategy that relies on a *finite* number of phase-space points (together with enough Stern-Gerlach repetitions N_r) in order to recover the full phase-space function as a linear combination of spherical harmonics.

C. Full tomography of phase-space functions

The full tomography of a phase-space function relies on multiple pointwise tomographies. Assuming that enough repetitions N_r of the Stern-Gerlach measurements are performed for each phase-space point, the corresponding spherical-harmonics coefficients can then be obtained from pointwise tomographies for a *finite* number of phase-space points [90, 103]. One straight-forward method to determine the spherical-harmonics decomposition of a spin- J function is by performing pointwise tomographies via Result 3 on an equiangular grid of at least $(4J+2)^2$ phase-space points (or combinations of rotation angles). (This does *not* imply a general lower bound and other measurement strategies might be able to use fewer than $(4J+2)^2$ phase-space points.) In this case, one can apply the sampling technique described in [103, Theorem 3] and [90, Theorem 7.1], which determines a phase-space function as a linear combination of spherical harmonics. The equiangular grid is given by at least $(4J+2)^2$ combinations of rotation angles $\theta_k = (\pi k)/N_p$ and $\phi_q = (2\pi q)/N_p$ for $k, q \in \{0, \dots, N_p - 1\}$ and $N_p \geq 4J+2$.

Result 4. *The complete phase-space function $F_\rho(\Omega, s) = \sum_{j=0}^{2J} \sum_{m=-j}^j c_{jm} Y_{jm}(\Omega)$ is determined by its spherical-harmonics expansion coefficients c_{jm} which are computed from phase-space reconstructions $\tilde{F}_\rho(\theta_k, \phi_q, s)$ at*

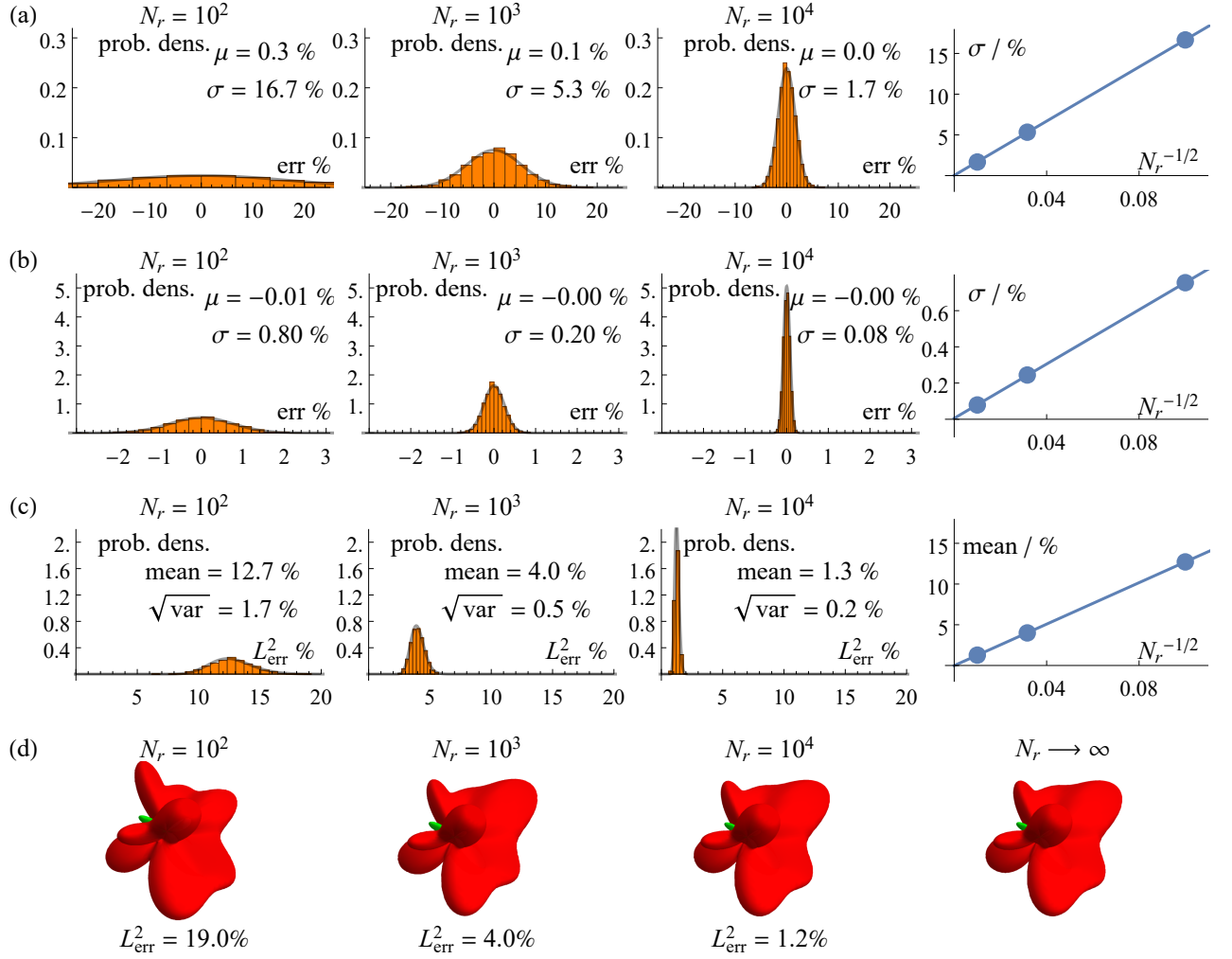


FIG. 6. Simulated tomography of Wigner functions $W_\rho(\theta, \phi)$ for a random ensemble of $N_\rho = 2200$ spin-5/2 states ρ : (a) Pointwise tomography at the phase-space point $(\theta, \phi) = (0, 0)$ as discussed in Sec. IV A. The relative reconstruction errors (relative to the global maximum of the ideal phase-space function) empirically follow a Gaussian distribution. Its mean μ and standard deviation σ are obtained from a fitted Gaussian distribution. And σ empirically scales as $N_r^{-1/2}$ with the number N_r of repetitions. (b) Pointwise tomographies from (a) evaluated at $22^2 = 484$ phase-space points (as discussed in Sec. IV B) for points (θ_k, ϕ_q) from an equiangular grid (refer to Sec. IV C). The relative reconstruction errors (relative to the global maximum of the ideal phase-space function) are averaged over the grid points (θ_k, ϕ_q) . The mean μ and standard deviation σ of the average error are obtained from a fitted Gaussian distribution; σ empirically scales as $N_r^{-1/2}$. (c) Full tomography as discussed in Sec. IV C using an equiangular grid of $22^2 = 484$ phase-space points. The relative L^2 -norm errors (relative to the global maximum of the ideal phase-space function) empirically follow a log-normal distribution. The mean and standard deviation is determined from a fitted log-normal distribution and the mean also scales as $N_r^{-1/2}$. (d) Examples of reconstructed Wigner functions from (c) with their relative L^2 -norm errors.

the phase-space points (or angles) (θ_k, ϕ_q) as

$$c_{jm} = \frac{2\pi\sqrt{2}}{N_p} \sum_{k=0}^{N_p-1} \sum_{q=0}^{N_p-1} \alpha_k^{(N_p)} \tilde{F}_\rho(\theta_k, \phi_q, s) [Y_{jm}(\theta_k, \phi_q)]^*.$$

A closed formula for the real coefficients $\alpha_k^{(N_p)}$ can be found in [90, 103]. Increasing the number N_p beyond its lower bound $4J+2$ might help to reduce errors due to experimental imperfections in precisely setting the rotation angles. Note that the pointwise reconstructions $\tilde{F}_\rho(\theta_k, \phi_q, s)$ are usually susceptible to shot noise (due to

the finite number N_r of Stern-Gerlach repetitions) and this also affects the full tomography of the phase-space function. In Fig. 6 (c), the full tomography using Result 4 is simulated for a random ensemble of $N_\rho = 2200$ spin-5/2 quantum states. The reconstruction error is given as the relative L^2 -norm difference between the reconstructed and the ideal phase-space functions (relative to the ideal one) and it empirically follows a log-normal distribution. The mean of the reconstruction error empirically scales as $N_r^{-1/2}$ and vanishes as the number N_r of measurements increases.

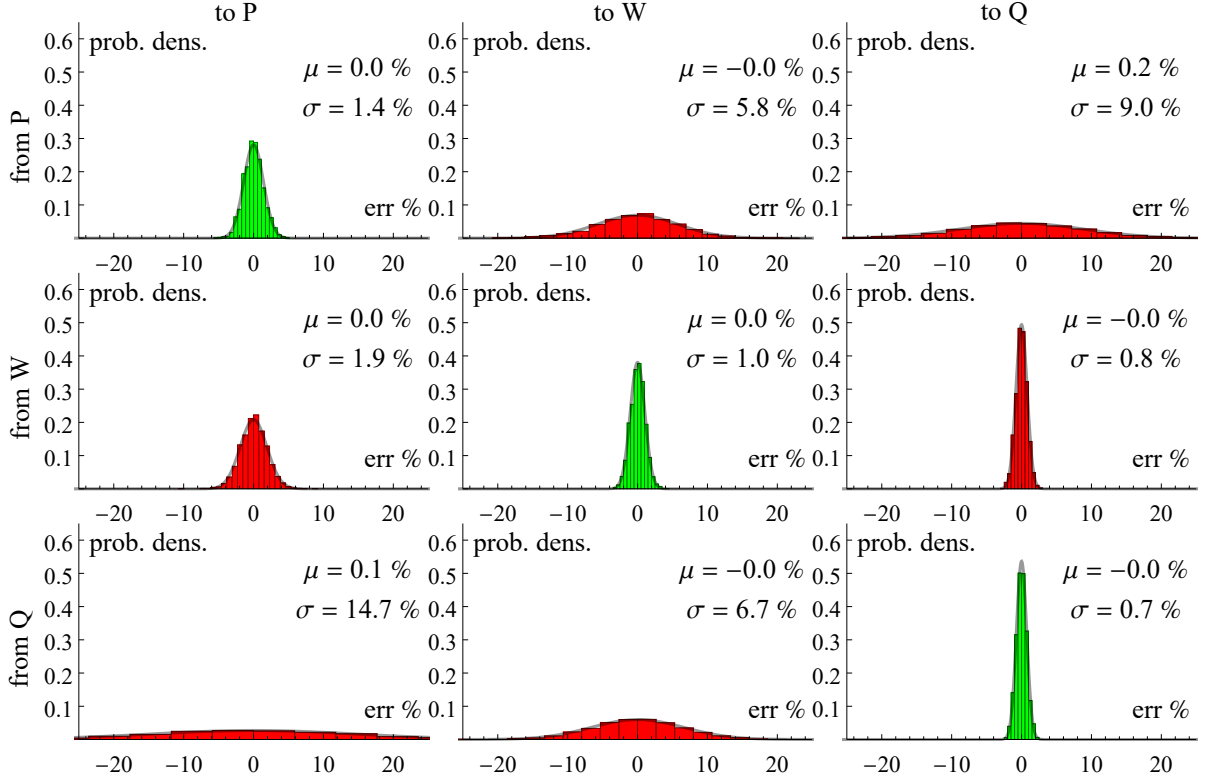


FIG. 7. Relative reconstruction errors (relative to the global maximum of the ideal phase-space function) of simulated full tomographies of P, W, and Q functions evaluated at the phase-space point $(\theta, \phi) = (0, 0)$ for a random ensemble of $N_\rho = 2200$ spin-5/2 states using $N_r = 1000$ Stern-Gerlach repetitions. This is similar as discussed in Sec. IV C but the reconstruction errors are only evaluated at $(\theta, \phi) = (0, 0)$. The directly reconstructed phase-space functions (cf. Result 4) for the green histograms on the diagonal are in a second step transformed with a spherical convolution (cf. Result 2) to P, W, and Q functions for the red, off-diagonal histograms. The direct reconstruction is usually preferable. The mean μ and standard deviation σ are obtained from a fitted Gaussian distribution.

Obviously, Result 4 describes only one of many measurement strategies that can be envisioned by starting from Result 3. In particular, Result 4 uses an equiangular grid and results in a concentration of sampling points at the poles. More isotropic measurement strategies can rely on (e.g.) Lebedev grids [104–106]. A more detailed and thorough discussion of suitable measurement strategies is left to future research. In the remaining parts of Sec. IV, we discuss certain drawbacks of combining a tomography with a spherical convolution as well as various connections to related work. Finally, we close this section with a discussion in Sec. IV G.

D. Drawbacks of combining a tomography with a spherical convolution

A reduced number N_r of Stern-Gerlach repetitions might lead to a substantial error when one transforms a reconstructed phase-space function to a different member of the s -parametrized class of phase-space functions using a spherical convolution (see Result 2). Figure 7 details this effect for simulated full tomographies (see Sec. IV C) of P, W, and Q functions evaluated at the phase-space

point $(\theta, \phi) = (0, 0)$. The stated relative errors are given by the difference between the simulated full reconstruction and the ideal phase-space function (relative to the global maximum of the ideal one). First, Result 4 is used for a full tomography of $N_\rho = 2200$ random spin-5/2 states, where $N_r = 1000$ Stern-Gerlach repetitions are considered. This results in the green histograms on the diagonal of Fig. 7. Second, the reconstructed complete phase-space functions are transformed to P, W, and Q functions by applying Result 2. One obtains the red, off-diagonal histograms in Fig. 7.

Similarly, Fig. 8 considers the full tomography (see Sec. IV C) and shows simulated histograms for the relative L^2 -norm errors between the ideal and the reconstructed phase-space functions (relative to the L^2 norm of the ideal one). The red, off-diagonal parts for both Figure 7 and 8 highlight that one should usually avoid an indirect approach that combines a tomography with a spherical convolution from Result 2, at least for a reduced number N_r of Stern-Gerlach repetitions. A direct tomography of the desired class of s -parametrized phase-space function using Result 3 or Result 4 is preferable. This highlights that not all reconstruction strategies are

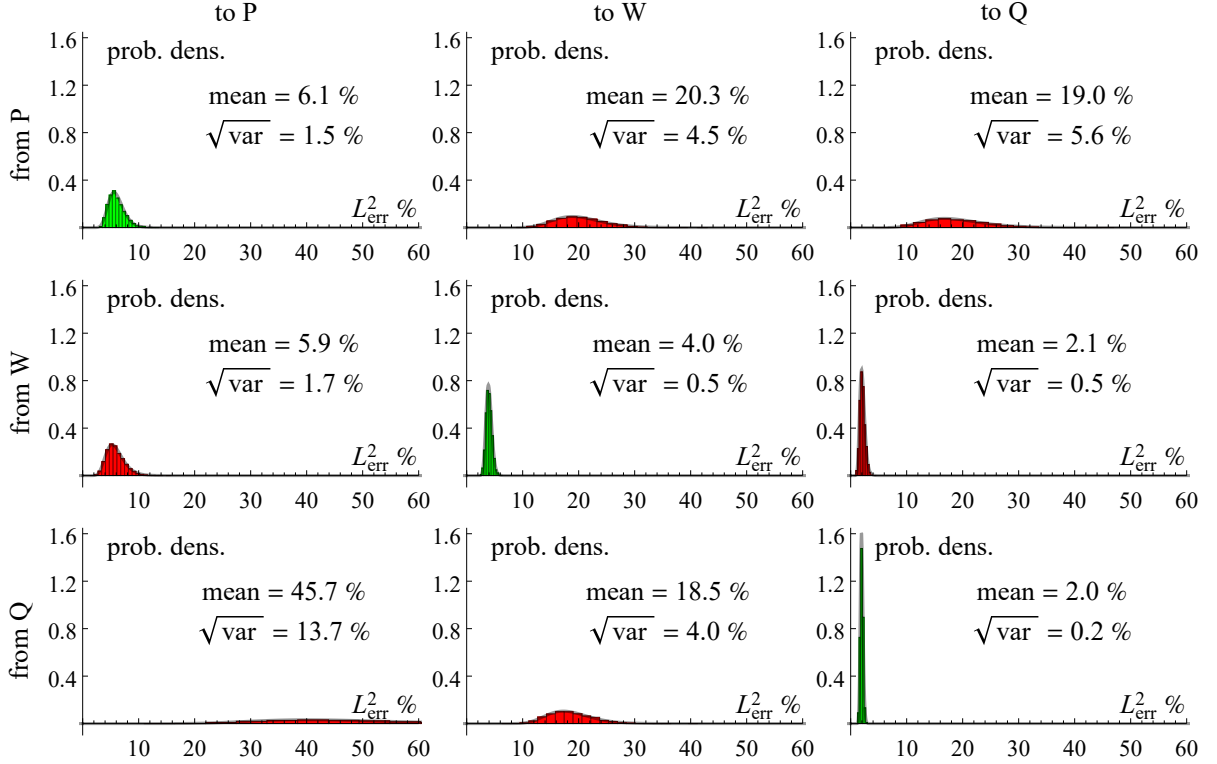


FIG. 8. Similar as in Fig. 7, the relative reconstruction errors are given here, however, for the full phase-space function as relative L^2 errors (and not only for a single phase-space point). The directly reconstructed phase-space functions for the green histograms on the diagonal are usually preferable to the red, off-diagonal histograms that are obtained from the green ones by applying an additional spherical convolution (see Result 2).

equally advisable under significant errors, even though the transformations in Result 2 are reversible if one neglects errors. We have limited our discussion to errors which are a consequence of having only a finite number of Stern-Gerlach repetitions at each phase-space point.

E. Related Experimental Work

Similar tomography approaches for the reconstruction of phase-space functions that emphasize rotational symmetries of finite-dimensional quantum systems and rely on rotated parity operators (as in Result 3) have been experimentally validated in the literature [63, 107, 108]. In [63], Stern-Gerlach measurements have been performed in order to determine the probabilities of finding a quantum system in rotated basis states, and this allowed them to experimentally recover a particular type of a multi-spin phase-space function that arises from products of single-spin phase-space functions (refer to [62] as discussed in Sec. III A). The nuclear magnetic resonance experiments in [107] did not rely on Stern-Gerlach measurements, but directly measured the overlaps between the mixed quantum state and rotated axial tensor operators, where generalized multi-spin Wigner functions [80] have been experimentally reconstructed without first recover-

ing the density matrix. The approach of [107] has been recently also applied to the experimental reconstruction of propagators and quantum gates [108]. These experiments highlight the convenience of incorporating rotations directly in the tomography scheme as we have done in Result 3 for the whole class of s -parametrized phase-space functions, which includes the Glauber P, Wigner, and Husimi Q function.

Let us also compare our work to the ‘filtered backprojection’ technique in Sec. 2 of [30] (which differs from the spherical Radon approach in Sec. IV F also discussed in [30]): it relies on the experiments in [29] and recovers a Wigner function from a finite number N of Stern-Gerlach measurements (each performed in a rotated reference frame Ω_n): The Wigner functions $W_{|m_n\rangle}$ of the projection eigenstates $|m_n\rangle$ are inversely rotated and summed up as $\sum_{n=1}^N c_n \mathcal{R}^{-1}(\Omega_n)[W_{|m_n\rangle}]$. A subsequent spherical convolution with a filter function reconstructs the Wigner function in [30], which is in the limit of infinite and evenly distributed measurements agrees with the general Result 3. In addition, Result 3 does not rely on a spherical convolution and enables diverse reconstruction strategies as the distribution function $F_\rho(\Omega, s)$ can be independently determined for each phase-space point Ω .

Our comparison to related experimental work clearly shows the feasibility of our tomography scheme and the

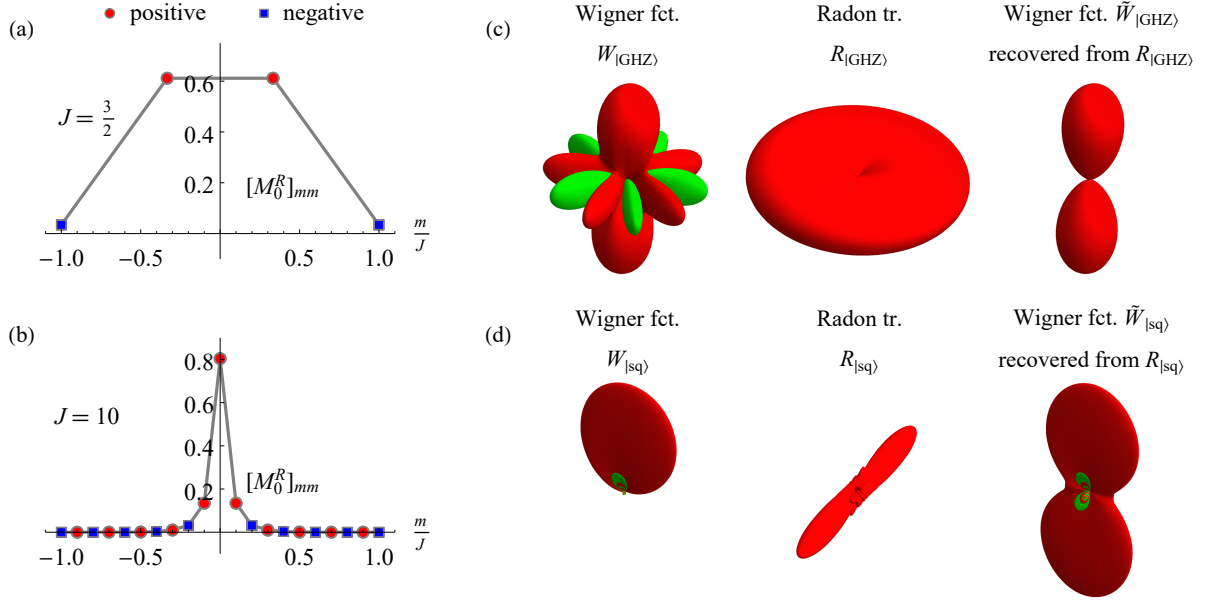


FIG. 9. (a)-(b) Stern-Gerlach reconstruction weights $[M_0^R]_{mm}$ in Eq. (13) for the Radon transform of a Wigner function applicable to a single spin J (cf. Fig. 3); (c)-(d) Wigner function (cf. Fig. 5), its Radon transform, and its point-symmetric part reconstructed by inverse Radon transformation: (c) quantum state of a single spin with $J = 5/2$ corresponding to the GHZ state of $2J$ qubits (cf. Fig. 5(a)), (d) squeezed state $|\text{sq}\rangle$ of a single spin with $J = 10$ (cf. Fig. 5(b)) approximately localized on the upper hemisphere of its Wigner function $W_{|\text{sq}\rangle}$, the corresponding Radon transform $R_{|\text{sq}\rangle}$ is highly localized around the equator and can be reconstructed using few measurements. Red (dark gray) and green (light gray) represent positive and negative values, respectively.

use of rotated parity operators appropriately reflects the rotational symmetries of finite-dimensional quantum systems. Consequently, we believe that our tomography scheme will be beneficial for a large class of experimental scenarios.

F. Comparison to the spherical Radon approach

We also relate Result 3 to optical homodyne tomography [43, 44, 109] (cf. Eq. (6.12) in [57]) and especially to the finite-dimensional case as discussed in [30]. The planar Radon transformation of a Wigner function is replaced in finite dimensions with the spherical Radon transformation, which is the integral along the great circle orthogonal to the vector pointing to a phase-space point Ω [89]. Refer to Fig. 9 for plots of the Radon transforms $R_{|\text{GHZ}\rangle}$ and $R_{|\text{sq}\rangle}$ of Wigner functions for a GHZ state and a squeezed state, respectively. The Radon transforms of Wigner functions can be directly obtained from the Stern-Gerlach probabilities $p_m(\Omega)$ by replacing the weights in Eq. (12) with the relevant parity operators $[M_0^R]_{mm}$ [see Fig. 9(a)-(b)]. One has

$$M_s^R := \sum_{j=0}^{2J} \sqrt{\frac{2j+1}{4\pi}} P_j(0) (\gamma_j)^{-s} T_{j0} \quad (13)$$

for general s -parametrized phase-space representations where the Legendre polynomial $P_j(0)$ [89] is used. The

point-symmetric parts $\tilde{W}_{|\text{GHZ}\rangle}$ and $\tilde{W}_{|\text{sq}\rangle}$ of the Wigner functions are recovered via an inverse spherical Radon transform [right of Fig. 9(c)-(d)]. In general, one does however *not* recover the complete Wigner function using this approach, compare, e.g., the left and right part of Fig. 9(c). But in typical experiments with large J , the Wigner function is localized around the north pole and measuring probabilities $p_m(\Omega)$ close to the equator still allows for its reconstruction from its Radon transform [middle of Fig. 9(d)] by assuming a point-symmetric Wigner function [right of Fig. 9(d)], which—in this particular case—still contains the full information of the quantum state, cf. Sec. 3 in [30]. The great-circle integrals for the spherical Radon transform converge to the usual line integrals of the planar Radon transformation.

One concludes that the spherical Radon approach is *not* suitable to recover general states of a finite-dimensional quantum system due to essential geometric limitations of the spherical Radon transform. This clarifies that not all infinite-dimensional tomography schemes (as the Radon approach [43, 44, 57, 109]) lead to unproblematic approaches when restricted to finite dimensions.

G. Other aspects and discussion

As for infinite-dimensional phase-space methods (cf. Eq. (6.8) in [7]), one can also use our approach to re-

construct the density matrix (which, however, is not the subject of this work)

$$\rho = \int_{S^2} F_\rho(\Omega, s) \mathcal{R}(\Omega) M_{-s} \mathcal{R}^\dagger(\Omega) d\Omega, \quad (14)$$

from its phase-space representation by inverting Result 1 with a spherical integration. Note that the reconstruction from the Q function is more precarious as M_1 diverges for large J . A tomography formula

$$\rho = \sum_{m=-J}^J [M_s]_{mm} \int_{S^2} p_m(\Omega) \mathcal{R}(\Omega) M_{-s} \mathcal{R}^\dagger(\Omega) d\Omega \quad (15)$$

in terms of the Stern-Gerlach probabilities $p_m(\Omega)$ is obtained by combining Eqs. (12) and (14), where the integrals can be numerically estimated from finitely many spherical samples via (e.g.) Gaussian quadratures [90]. This generalizes [101, 110, 111], and the ‘filtered back-projection’ technique for the density matrix (see Eq. (9) in [30]) agrees in the limit of infinite measurements with Eq. (15).

While a majority of earlier work focuses on reconstructing density matrices or infinite-dimensional phase-space functions from measured data (see, e.g., [109, 112–118]), we have presented in Eq. (12) of Result 3 a general tomography formula for finite-dimensional phase-space representations. Such a tomography formula has not been reported before for the full class of all (finite-dimensional) s -parametrized phase-space representations. Result 3 provides the foundation for engineering statistical estimators [119] for the reconstruction of finite-dimensional phase-space representations in future research, which minimize the necessary Stern-Gerlach measurements while guaranteeing robustness via precisely bounded confidence intervals and ensuring a physical estimate. And Result 4 provides a first step in this direction.

For designing better statistical estimators, the characterization of the type and relative size of specific systematic and random errors involved in a given experimental realization would be necessary and choosing a statistical estimator closely depends on assumptions made in a concrete experiment. Given a formula [as Eq. (12)] to compute a desired target, one can use point estimators (such as maximum likelihood estimators) or set estimators [119] to determine a target which ‘best’ fits to the measured data.

The analysis in Sec. IV F shows that not all formulas used in the literature produce the desired results, even before taking into account any statistical approach. We have along these lines focussed in this work on the aspect of finding suitable tomography formulas. Especially since related experimental work has validated similar tomography approaches relying on rotated parity operators (see Sec. IV E) and the statistical aspects are quite similar to the widely discussed cases of reconstructing density matrices or infinite-dimensional phase-space functions [109, 112–118]. In Secs. IV A–IV C, we have discussed the reconstruction errors that arise from having

only a finite number N_r of Stern-Gerlach repetitions (i.e. shot noise). The resulting errors are illustrated in Fig. 6 and they behave as expected. The errors decrease as the number N_r of repetitions increases. Beyond this first analysis, a more detailed discussion of statistical and robustness questions is left to future work. We want to only remark that reconstructing a Wigner function directly using Result 3 or Result 4 is—under noise—preferable to convolving/deconvolving noisy P or Q functions via Result 2 as convolutions are well known to be sensitive to noise (cf. [48, 57]). This claim is also substantiated by simulations of Stern-Gerlach tomographies in Sec. IV D where the corresponding reconstruction errors are also determined. Therefore, not all reconstruction strategies are equally advisable under experimental noise as detailed in Figs. 7 and 8. Concrete experiments will have to be explicitly designed depending on characteristics of the desired final (phase-space) representation.

V. CONCLUSION

We have developed a unified formalism for spherical phase-space representations of finite-dimensional quantum states based on rotated parity operators. The rotated parity operators appropriately reflect the rotational symmetries of finite-dimensional quantum systems and the Stern-Gerlach frequencies (or related overlaps) from Eq. (11) are easily measured in experiments (see Sec. IV E). In addition, all of our results apply to the full class of (finite-dimensional) s -parametrized phase-space representations. We have (a) systematically defined spherical phase spaces for spin systems which recover the planar phase spaces from quantum optics in the large spin limit; (b) different types of phase-space representations can be translated into each other by convolving with spin-up state representations; (c) tomographic approaches can be now formulated consistently for all (finite-dimensional) s -parametrized phase-space representations; (d) the spherical Radon approach is not suitable to recover general states of finite-dimensional quantum systems. Our results pave the way for innovative tomography schemes to reconstruct phase-space functions of finite-dimensional quantum states.

ACKNOWLEDGMENTS

The authors are especially grateful to Thomas Schulte-Herbrüggen, Markus Grassl, Mark J. Everitt, and Lukas Knips for discussions and comments. B.K. acknowledges financial support from the scholarship program of the Bavarian Academic Center for Central, Eastern and Southeastern Europe (BAYHOST) and funding from the EU H2020-FETFLAG-03-2018 under grant agreement No 820495 (AQTION). R.Z. and S.J.G. acknowledge support from the Deutsche Forschungsgemeinschaft through Grant No. Gl 203/7-2. This work is supported

in part by the Elitenetzwerk Bayern through ExQM and the Deutsche Forschungsgemeinschaft (DFG, German Research Foundation) under Germany's Excellence

Strategy – EXC-2111 – 39081486. R.Z. acknowledges funding from the EU H2020-FETFLAG-03-2018 under grant agreement No 817482 (PASQuanS).

-
- [1] W. P. Schleich, *Quantum Optics in Phase Space* (Wiley-VCH, Berlin, 2001).
 - [2] C. K. Zachos, D. B. Fairlie, and T. L. Curtright, *Quantum Mechanics in Phase Space: An Overview with Selected Papers* (World Scientific, Singapore, 2005).
 - [3] F. E. Schroeck Jr., *Quantum Mechanics on Phase Space* (Springer, Dordrecht, 2013).
 - [4] T. L. Curtright, D. B. Fairlie, and C. K. Zachos, *A Concise Treatise on Quantum Mechanics in Phase Space* (World Scientific, Singapore, 2014).
 - [5] R. J. Glauber, Phys. Rev. **131**, 2766 (1963).
 - [6] R. J. Glauber, Rev. Mod. Phys. **78**, 1267 (2006).
 - [7] K. E. Cahill and R. J. Glauber, Phys. Rev. **177**, 1882 (1969).
 - [8] H. Groenewold, Physica **12**, 405 (1946).
 - [9] J. E. Moyal, Proc. Camb. Phil. Soc. **45**, 99 (1949).
 - [10] F. Bayen, M. Flato, C. Fronsdal, A. Lichnerowicz, and D. Sternheimer, Ann. Phys. **111**, 61 (1978).
 - [11] F. Bayen, M. Flato, C. Fronsdal, A. Lichnerowicz, and D. Sternheimer, Ann. Phys. **111**, 111 (1978).
 - [12] F. A. Berezin, Mathematics of the USSR-Izvestiya **8**, 1109 (1974).
 - [13] F. A. Berezin, Comm. Math. Phys. **40**, 153 (1975).
 - [14] H. Weyl, Z. Phys. **46**, 1 (1927).
 - [15] H. Weyl, *Gruppentheorie und Quantenmechanik*, 2nd ed. (Hirzel, Leipzig, 1931) english translation in [16].
 - [16] H. Weyl, *The Theory of Groups & Quantum Mechanics*, 2nd ed. (Dover Publ., New York, 1950).
 - [17] M. de Gosson, *The Wigner Transform* (World Scientific, London, 2017).
 - [18] M. A. de Gosson, “Born-Jordan Quantization: Theory and Applications,” (Springer, Switzerland, 2016) pp. 113–127.
 - [19] K. Gröchenig, *Foundations of Time-Frequency Analysis* (Birkhäuser, Boston, 2001).
 - [20] L. Cohen, J. Math. Phys. **7**, 781 (1966).
 - [21] L. Cohen, *Time-Frequency Analysis* (Prentice-Hall, Englewood Cliffs, NJ, 1995).
 - [22] R. McConnell, H. Zhang, J. Hu, S. Ćuk, and V. Vuletić, Nature **519**, 439 (2015).
 - [23] F. Haas, J. Volz, R. Gehr, J. Reichel, and J. Estève, Science **344**, 180 (2014).
 - [24] M. H. Anderson, J. R. Ensher, M. R. Matthews, C. E. Wieman, and E. A. Cornell, Science **269**, 198 (1995).
 - [25] T.-L. Ho, Phys. Rev. Lett. **81**, 742 (1998).
 - [26] T. Ohmi and K. Machida, J. Phys. Soc. Jpn. **67**, 1822 (1998).
 - [27] J. Stenger, S. Inouye, D. Stamper-Kurn, H.-J. Miesner, A. Chikkatur, and W. Ketterle, Nature **396**, 345 (1998).
 - [28] Y.-J. Lin, K. Jiménez-García, and I. Spielman, Nature **471**, 83 (2011).
 - [29] M. F. Riedel, P. Böhi, Y. Li, T. W. Hänsch, A. Sinatra, and P. Treutlein, Nature **464**, 1170 (2010).
 - [30] R. Schmied and P. Treutlein, New J. Phys. **13**, 065019 (2011).
 - [31] C. D. Hamley, C. S. Gerving, T. M. Hoang, E. M. Bookjans, and M. S. Chapman, Nat. Phys. **8**, 305 (2012).
 - [32] H. Strobel, W. Muessel, D. Linnemann, T. Zibold, D. B. Hume, L. Pezzè, A. Smerzi, and M. K. Oberthaler, Science **345**, 424 (2014).
 - [33] D. Leibfried, E. Knill, S. Seidelin, J. Britton, R. B. Blakestad, J. Chiaverini, D. B. Hume, W. M. Itano, J. D. Jost, C. Langer, R. Reichle, and D. J. Wineland, Nature **438**, 639 (2005).
 - [34] J. G. Bohnet, B. C. Sawyer, J. W. Britton, M. L. Wall, A. M. Rey, M. Foss-Feig, and J. J. Bollinger, Science **352**, 1297 (2016).
 - [35] T. Monz, P. Schindler, J. T. Barreiro, M. Chwalla, D. Nigg, W. A. Coish, M. Harlander, W. Hänsel, M. Hennrich, and R. Blatt, Phys. Rev. Lett. **106**, 130506 (2011).
 - [36] F. Bouchard, P. de la Hoz, G. Bjork, R. W. Boyd, M. Grassl, Z. Hradil, E. Karimi, A. Klimov, G. Leuchs, J. Rehacek, and L. L. Sanchez-Soto, Optica **4**, 1429 (2017).
 - [37] A. B. Klimov, M. Zwiernik, S. Wallentowitz, M. Jarzyna, and K. Banaszek, New J. Phys. **19**, 073013 (2017).
 - [38] S. Chaturvedi, G. Marmo, N. Mukunda, R. Simon, and A. Zampini, Rev. Math. Phys. **18**, 887 (2006).
 - [39] W. K. Wootters, Ann. Phys. **176**, 1 (1987).
 - [40] U. Leonhardt, Phys. Rev. A **53**, 2998 (1996).
 - [41] K. S. Gibbons, M. J. Hoffman, and W. K. Wootters, Phys. Rev. A **70**, 062101 (2004).
 - [42] C. Ferrie and J. Emerson, New J. Phys. **11**, 063040 (2009).
 - [43] U. Leonhardt, *Measuring the Quantum State of Light* (Cambridge Univ. Press, Cambridge, 1997).
 - [44] D. T. Smithey, M. Beck, M. G. Raymer, and A. Fardani, Phys. Rev. Lett. **70**, 1244 (1993).
 - [45] K. Husimi, Proc. Phys. Math. Soc. Japan **22**, 264 (1940).
 - [46] J. Kanem, S. Maneshi, S. Myrskog, and A. Steinberg, J. Opt. B **7**, S705 (2005).
 - [47] C. Eichler, D. Bozyigit, C. Lang, L. Steffen, J. Fink, and A. Wallraff, Phys. Rev. Lett. **106**, 220503 (2011).
 - [48] G. S. Agarwal, Phys. Rev. A **57**, 671 (1998).
 - [49] B. Koczor, R. Zeier, and S. J. Glaser, J. Phys. A. **52**, 055302 (2019).
 - [50] R. H. Dicke, Phys. Rev. **93**, 99 (1954).
 - [51] J. K. Stockton, J. M. Geremia, A. C. Doherty, and H. Mabuchi, Phys. Rev. A **67**, 022112 (2003).
 - [52] G. Tóth, W. Wieczorek, D. Gross, R. Krischek, C. Schwemmer, and H. Weinfurter, Phys. Rev. Lett. **105**, 250403 (2010).
 - [53] B. Lücke, J. Peise, G. Vitagliano, J. Arlt, L. Santos, G. Tóth, and C. Klempt, Phys. Rev. Lett. **112**, 155304 (2014).
 - [54] W. Dür, G. Vidal, and J. I. Cirac, Phys. Rev. A **62**, 062314 (2000).
 - [55] J. J. Sakurai, *Modern Quantum Mechanics*, rev. ed. (Addison-Wesley, Reading, 1994).

- [56] J. Schwinger, in *Quantum Theory of Angular Momentum*, edited by L. C. Biedenharn and H. Van Dam (Academic Press, New York, 1965) pp. 229–279.
- [57] C. Brif and A. Mann, Phys. Rev. A **59**, 971 (1999).
- [58] G. S. Agarwal, Phys. Rev. A **24**, 2889 (1981).
- [59] J. P. Dowling, G. S. Agarwal, and W. P. Schleich, Phys. Rev. A **49**, 4101 (1994).
- [60] S. Heiss and S. Weigert, Phys. Rev. A **63**, 012105 (2000).
- [61] A. B. Klimov and H. de Guise, J. Phys. A **43**, 402001 (2010).
- [62] T. Tilma, M. J. Everitt, J. H. Samson, W. J. Munro, and K. Nemoto, Phys. Rev. Lett. **117**, 180401 (2016).
- [63] R. P. Rundle, P. W. Mills, T. Tilma, J. H. Samson, and M. J. Everitt, Phys. Rev. A **96**, 022117 (2017).
- [64] R. P. Rundle, T. Tilma, J. H. Samson, V. M. Dwyer, R. F. Bishop, and M. J. Everitt, **99**, 012115 (2019).
- [65] J.-P. Gazeau, *Coherent States in Quantum Physics* (Wiley-VCH, Weinheim, 2009).
- [66] H. Moya-Cessa and P. L. Knight, Phys. Rev. A **48**, 2479 (1993).
- [67] B. Koczor, F. vom Ende, M. A. de Gosson, S. J. Glaser, and R. Zeier, “Phase Spaces, Parity Operators, and the Born-Jordan Distribution,” (2018), (*Preprint arXiv:1811.05872*).
- [68] A. Grossmann, Comm. Math. Phys. **48**, 191 (1976).
- [69] A. Messiah, *Quantum Mechanics II* (North-Holland Publishing Company, Amsterdam, 1962).
- [70] A. Perelomov, *Generalized Coherent States and Their Applications* (Springer, Berlin, 2012).
- [71] F. Arecchi, E. Courtens, R. Gilmore, and H. Thomas, Phys. Rev. A **6**, 2211 (1972).
- [72] G. Racah, Phys. Rev. **62**, 438 (1942).
- [73] B. Koczor, *On phase-space representations of spin systems and their relations to infinite-dimensional quantum states*, Dissertation, Technische Universität München, Munich (2019).
- [74] J.-P. Amiet and S. Weigert, Phys. Rev. A **63**, 012102 (2000).
- [75] A. B. Klimov, J. L. Romero, and H. de Guise, J. Phys. A **50**, 1 (2017).
- [76] R. Stratonovich, Sov. Phys. D **1**, 414 (1956).
- [77] J. C. Várilly and J. M. Garcia-Bondía, Ann. Phys. **190**, 107 (1989).
- [78] B. Koczor, R. Zeier, and S. J. Glaser, Ann. Phys. **408**, 1 (2019).
- [79] T. Tilma and K. Nemoto, J. Phys. A **45**, 015302 (2012).
- [80] A. Garon, R. Zeier, and S. J. Glaser, Phys. Rev. A **91**, 042122 (2015).
- [81] C. Brif and A. Mann, J. Phys. A **31**, L9 (1997).
- [82] L. C. Biedenharn and J. D. Louck, *Angular Momentum in Quantum Physics* (Addison-Wesley, Reading, MA, 1981).
- [83] U. Fano, Phys. Rev. **90**, 577 (1953).
- [84] N. Tajima, Phys. Rev. C **91**, 014320 (2015).
- [85] X. M. Feng, P. Wang, W. Yang, and G. R. Jin, Phys. Rev. E **92**, 043307 (2015).
- [86] A. R. Usha Devi, Shudha, and A. K. Rajagopal, Quantum Inf. Process. **11**, 685 (2012).
- [87] G. Björk, A. B. Klimov, P. de la Hoz, M. Grassl, G. Leuchs, and L. L. Sánchez-Soto, Physical Review A **92**, 031801 (2015).
- [88] O. Giraud, P. Braun, and D. Braun, Phys. Rev. A **78**, 042112 (2008).
- [89] H. Groemer, *Geometric Applications of Fourier Series and Spherical Harmonics* (Cambridge University Press, Cambridge, 1996).
- [90] R. A. Kennedy and P. Sadeghi, *Hilbert Space Methods in Signal Processing* (Cambridge University Press, Cambridge, 2013).
- [91] V. Bužek, C. H. Keitel, and P. L. Knight, Phys. Rev. A **51**, 2594 (1995).
- [92] T. Opatrny, V. Bužek, J. Bajer, and G. Drobný, Phys. Rev. A **52**, 2419 (1995).
- [93] Keihänen, E. and Reinecke, M., Astron. Astrophys. **548**, A110 (2012).
- [94] B. D. Wandelt and K. M. Górski, Phys. Rev. D **63**, 123002 (2001).
- [95] The depicted random pure state vector is approximately given by $(0.06 + i0.02, -0.21 - i0.19, 0.04 + i0.27, 0.15 - i0.11, 0.28 - i0.28, -0.33 - i0.25, 0.04 - i0.44, -0.21 - i0.24, -0.43 + i0.00)^T$.
- [96] J. Ma, X. Wang, C.-P. Sun, and F. Nori, Phys. Rep. **509**, 89 (2011).
- [97] S. Deleglise, I. Dotsenko, C. Sayrin, J. Bernu, M. Brune, J.-M. Raimond, and S. Haroche, Nature **455**, 510 (2008).
- [98] L. G. Lutterbach and L. Davidovich, Phys. Rev. Lett. **78**, 2547 (1997).
- [99] P. Bertet, A. Auffeves, P. Maioli, S. Osnaghi, T. Meunier, M. Brune, J. M. Raimond, and S. Haroche, Phys. Rev. Lett. **89**, 200402 (2002).
- [100] K. Banaszek, C. Radzewicz, K. Wódkiewicz, and J. S. Krasiński, Phys. Rev. A **60**, 674 (1999).
- [101] V. I. Man’ko and O. V. Man’ko, J. Exp. Theor. Phys. **85**, 430 (1997).
- [102] K. Życzkowski, K. A. Penson, I. Nechita, and B. Collins, J. Math. Phys. **52**, 062201 (2011).
- [103] J. R. Driscoll and D. M. Healy, Adv. Appl. Math. **15**, 202 (1994).
- [104] V. I. Lebedev, USSR Comput. Math. & Math. Phys. **15**, 44 (1975).
- [105] V. I. Lebedev, USSR Comput. Math. & Math. Phys. **16**, 10 (1976).
- [106] V. I. Lebedev and D. N. Laikov, Russian Acad. Sci. Dokl. Math. **59**, 477 (1999).
- [107] D. Leiner, R. Zeier, and S. J. Glaser, Phys. Rev. A **96**, 063413 (2017).
- [108] D. Leiner and S. J. Glaser, Phys. Rev. A **98**, 012112 (2018).
- [109] M. Paris and J. Řeháček, eds., *Quantum State Estimation* (Springer, Berlin, 2004).
- [110] J.-P. Amiet and S. Weigert, J. Phys. A **31**, L543 (1998).
- [111] G. D’Ariano, L. Maccone, and M. Paini, J. Opt. B **5**, 77 (2003).
- [112] C. Schwemmer, L. Knips, D. Richart, H. Weinfurter, T. Moroder, M. Kleinmann, and O. Gühne, Phys. Rev. Lett. **114**, 080403 (2015).
- [113] L. Knips, C. Schwemmer, N. Klein, J. Reuter, G. Tóth, and H. Weinfurter, “How long does it take to obtain a physical density matrix?” (2015), arXiv:1512.06866v1.
- [114] P. Faist and R. Renner, Phys. Rev. Lett. **117**, 010404 (2016).
- [115] G. B. Silva, S. Glancy, and H. M. Vasconcelos, Phys. Rev. A **95**, 022107 (2017).
- [116] A. Steffens, C. A. Riofrí, W. McCutcheon, I. Roth, B. A. Bell, A. McMillan, M. S. Tame, J. G. Rarity, and J. Eis-

- ert, Quantum Sci. Technol. **2**, 025005 (2017).
- [117] C. A. Riofrí, D. Gross, S. T. Flammia, T. Monz, D. Nigg, R. Blatt, and J. Eisert, Nat. Commun. **8**, 15305 (2017).
- [118] D. Suess, L. Rudnicki, D. Gross, and T. O. Maciel, New J. Phys. **19**, 093013 (2017).
- [119] M. J. Schervish, *Theory of Statistics* (Springer, New York, 1995).